Available online at www.sciencedirect.com
ScienceDirect
Journal of Molecular Graphics and Modelling 25 (2006) 495–506
Journal of Molecular Graphics and Modelling
www.elsevier.com/locate/JMGM

Molecular dynamics simulations to aid the rational design of organic friction modifiers

J.E. Davidson [a,*], S.L. Hinchley [a], S.G. Harris [b], A. Parkin [a], S. Parsons [a], P.A. Tasker [a]

[a] School of Chemistry, The University of Edinburgh, West Mains Road, Edinburgh EH9 3JJ, United Kingdom
[b] Infineum UK Ltd., P.O. Box 1, Milton Hill, Abingdon, Oxfordshire OX13 6BB, United Kingdom

Received 22 November 2005; received in revised form 25 March 2006; accepted 25 March 2006
Available online 25 April 2006

Abstract

Molecular dynamics simulations were performed under conditions of constant volume and temperature and of constant pressure and temperature to elucidate the structure activity relationships of a series of non-ionic surfactant molecules derived from vegetable fat and employed as friction modifiers in commercial engine oils. The simulations show the extent to which intermolecular hydrogen bonding is important in determining the stability of the monolayer formed by the surfactant molecules and show that mono-alkanoyl glyceride molecules are able to pack more efficiently, forming significantly more intermolecular hydrogen bonds and occupying approximately half the volume needed by di-alkanoyl glyceride molecules. Density profiles are presented which show significant mixing of the hydrophobic tail groups and a non-polar solvent. The distribution of torsion angles in the tail groups shows that the conformation is consistent with a liquid at finite temperature rather than a crystal structure. The measured friction coefficients of equimolar solutions of the glycerides show that the efficacy as friction modifiers varies in the order mono-, di- and the tri-oleyl glyceride, which is consistent with the efficacy of film formation predicted by the molecular dynamics calculations.

Keywords: Molecular dynamics; Force field; Organic friction modifier (OFM); Fatty ester; Surface modification; Database mining

1. Introduction

Friction is defined as wear and energy loss between two moving surfaces [1]. In most parts of engines it is undesirable and the aim of lubrication is to minimise it as far as possible.

There are two types of friction: external friction which arises from microscopic contact points between two moving surfaces which can result in adhesion, deformation and grooving, and internal friction which arises from the viscosity of the lubricant. The relationship between them can be understood by looking at the Stribeck curve (Fig. 1). At the extreme left of the graph, the two metal surfaces are in direct contact with no lubricant between them. This is termed ''dry friction'' and is considered to be highly undesirable as it is associated with extremely high friction and wear. In the boundary friction region the two metal surfaces are separated by a monolayer of lubricant molecules. This is the region of greatest interest. The interactions are extremely complicated and poorly understood although it is believed that chemisorption and physisorption play an important role [1]. As the film between the two surfaces becomes gradually thicker the system enters the elastohydrodynamic region in which there are fewer and fewer metal–metal contacts as the lubricant film becomes progressively thicker. As the film becomes thicker the energy lost due to the lubricant viscosity, the internal friction, starts to increase so that eventually the friction coefficient passes through a minimum and starts to increase. Formulators designing additive packages would like to minimise both internal and external friction. This can be approached by using a friction modifier which will adsorb strongly onto a metal surface, thus providing good boundary and to a lesser extent elastohydrodynamic lubrication in combination with a low viscosity engine oil to reduce internal friction.

A common friction modifying additive is molybdenum dithiocarbamate (Fig. 2(A)) which decomposes in situ to generate molybdenum disulfide which has a graphite-like structure containing layers that can easily be sheared over each other [2]. This has proved to be an effective friction-reducing agent. Recently the manufacturers of lubricant additives have come under pressure from vehicle manufacturers and legislators to reduce the use of additives based on phosphorus, sulfur

* Corresponding author.
E-mail address: etive_beag@tiscali.co.uk (J.E. Davidson).

1093-3263/$ – see front matter
doi:10.1016/j.jmgm.2006.03.006

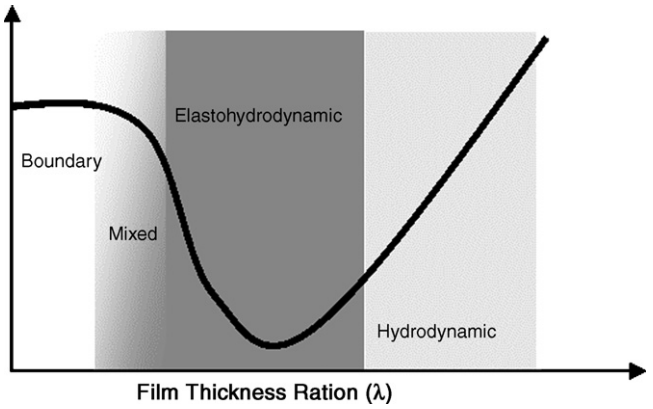

Fig. 1. The Stribeck curve illustrating the relationship between film thickness and friction coefficient.

and metals. In order to do this it is necessary to first understand the relationship between structure and activity of existing organic additives based on carbon, hydrogen and oxygen so that new additives can be designed.

The schematic structure of a friction modifier molecule is depicted in Fig. 2(B). The molecule has a polar head group (X in Fig. 2(B)) which interacts with the metal surfaces of engine components and a long alkyl tail group (R) to impart oil solubility.

These molecules are believed to reduce friction by adsorbing onto surfaces to generate friction-reducing layers (Fig. 3) [3]. The dependence of the strength of adsorption and efficacy of organic modifiers of the form shown in Fig. 2 on the nature of the head group (X) and tail group (R) has been investigated experimentally by Beltzer and Jahanmir [4–7].

It was proposed that the free energy of binding of this type of molecule is dependent on the surface coverage so the Temkin isotherm (Eq. (1)) was used [4–8].

$$\Delta G_{\text{ads}} = \Delta G_0 + \alpha\theta \tag{1}$$

where ΔG_{ads} is the energy of adsorption; θ the fractional surface coverage; α is a positive constant, dependent on the interaction of additive molecules at the surface.

A series of *n*-alkanoic carboxylic acids containing 12, 14, 16 and 18 carbon atoms was studied, and a linear decrease in friction coefficient with chain length was reported [6]. A correlation between efficacy as a friction modifier, chain length and enthalpy of fusion was reported and the authors proposed that the lower friction of the higher acids is due to stronger intermolecular (van der Waals) interactions between molecules in a surface film which make it harder to form a defect [6]. The melting points of some common fatty acids are listed in Appendix 1.

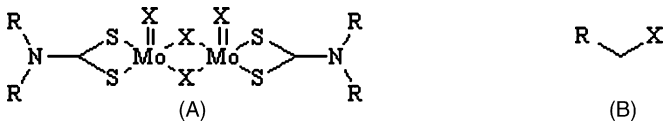

Fig. 2. (A) Molybdenum dithiocarbamate. X = O or S, R = alkyl chain of between four and eight carbon atoms in length. (B) Organic friction modifier, X represents the polar head group and R the hydrocarbon tail group.

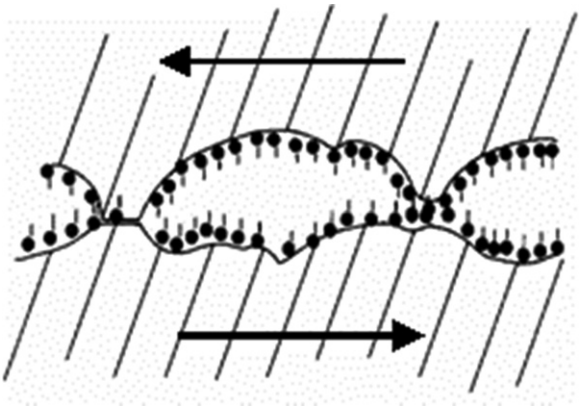

Fig. 3. Proposed mechanism of friction reduction by organic friction modifiers. The polar head groups are represented by circles and the apolar tail groups are represented by lines [3].

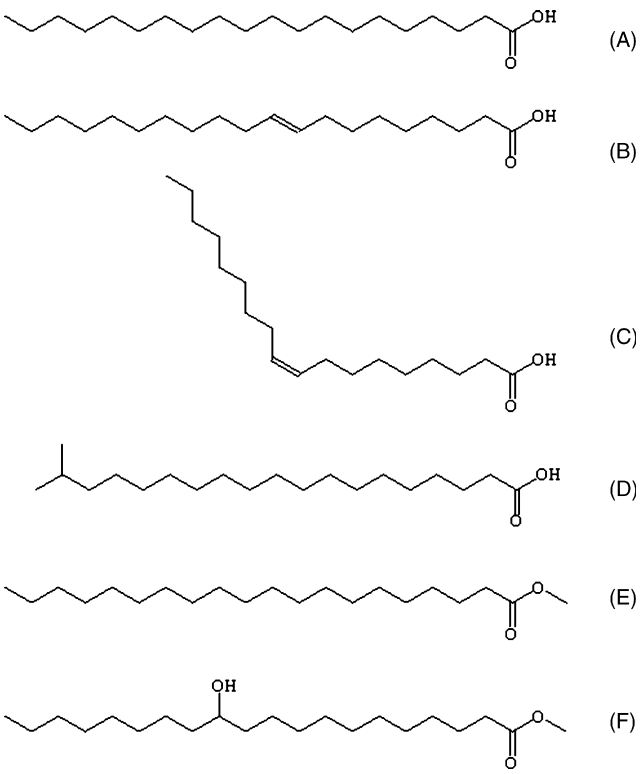

Fig. 4. Stearic acid (A), elaidic acid (B), oleic acid (C), isostearic acid (D), methyl stearate (E) and 12-hydroxy methyl stearate (F).

The effect of chain unsaturation in C_{18} carboxylic acids on the friction-reducing behaviour and adsorption characteristics was investigated by studying stearic, elaidic and oleic acids (Fig. 4). It was reported that stearic acid, which has a saturated alkyl chain,

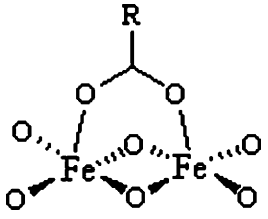

Fig. 5. Proposed method of binding of carboxylates to iron surfaces [9–11].

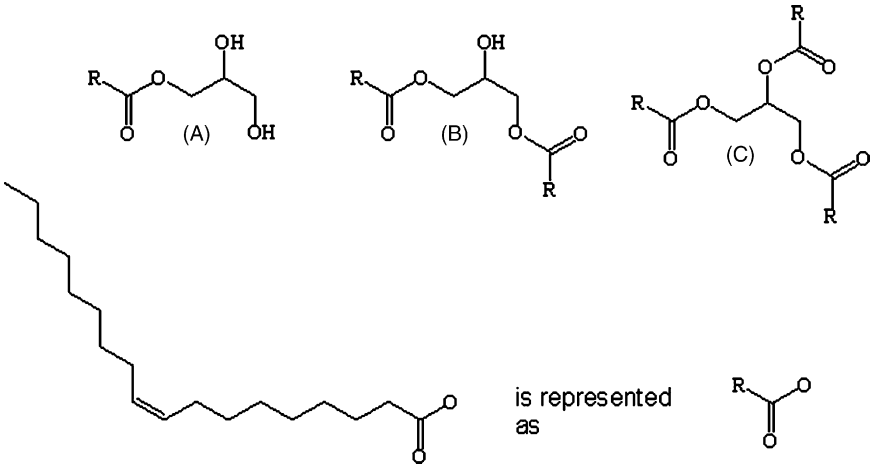

Fig. 6. (A) 1-Mono-oleyl glyceride (1-mog), (B) 1,3-di-oleyl glyceride (1,3-dog) and (C) tri-oleyl glyceride (tog).

is the most strongly surface active and gives the lowest friction coefficient [7]. Elaidic acid has a *trans* double bond in the centre of the tail group that disrupts the packing of the molecules and results in an increased friction coefficient [7]. Oleic acid has a *cis* double bond in the centre of the tail group which further disrupts the packing of the molecules at the surface and results in a greater friction coefficient than either stearic or oleic acid [7].

Comparison of the binding and friction-reducing properties of *n*-stearic and isostearic acid (Fig. 4(A and D)) showed that isostearic acid binds less strongly than *n*-stearic acid and is a less effective friction modifier. It was proposed that the methyl group disrupts the packing of the alkyl chains resulting in less efficient packing, weaker surface bonding and a higher friction coefficient relative to the unbranched *n*-stearic acid (Fig. 4) [4].

The effect of side groups on the chain, which might allow intermolecular hydrogen bonding, was studied by comparing 12-hydroxy methyl stearate and methyl stearate (Fig. 4(E and F)). 12-Hydroxy methyl stearate was found to bind more strongly and to be better at reducing friction than methyl stearate [4]. It was proposed that the hydroxyl group is able to form hydrogen bonds that stabilise the surface film [4]. It was also found that the ability of the head group to interact with the surface has an effect on binding strength, so that stearic acid which is able to deprotonate in order to form covalent bonds to the iron atoms in the surface (e.g. as in Fig. 5) is adsorbed more strongly than methyl stearate or stearyl alcohol which interact with the surface via hydrogen bonds [4,9–11].

The production of organic modifiers is based on complete hydrolysis of vegetable fats to give a mixture of glycerol and fatty acids and then partial dehydration to give a mixture of mono-, di- and tri-esters. Oleic acid is a significant component of vegetable oils (Appendix 2) and the predominant component of olive oil which is the main feedstock used in the production of OFMs [12]. The organic friction modifier (OFM) used by Infineum UK Ltd. (hereafter referred to as Infineum) is a mixture of mono-, di- and tri-alkanoyl glycerides.

1-Mono-oleyl glyceride (Fig. 6(A)), 1,3-di-oleyl glyceride (Fig. 6(B)) and tri-oleyl glyceride (Fig. 6(C)) were chosen to be representative of the principal components of organic friction modifiers.

The high frequency reciprocating rig (HFRR) apparatus shown in Fig. 7 was used to collect friction data. A steel ball is loaded against a flat plate and reciprocated back and forwards while immersed in friction modified oil. Data are shown in Fig. 8. The friction coefficient (μ) is defined as (Fig. 9) the ratio of frictional force (F) to normal force (N).

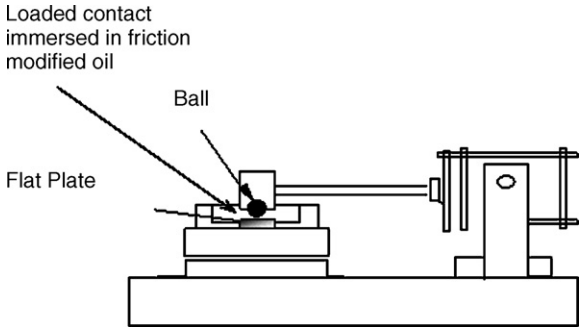

Fig. 7. High frequency reciprocating rig (HFRR) apparatus for the collection of friction and resistivity data by Infineum. The experimental conditions were: ball diameter 6 mm, load 4 N, frequency 20 Hz and stroke length 1 mm. Both ball and flat were of ANSI 52100 steel.

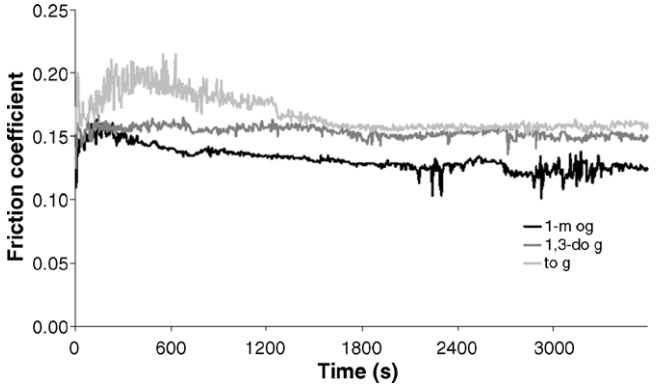

Fig. 8. Friction coefficients of 3.5×10^{-3} mol L^{-1} solutions of the three related oleyl glyceride molecules in a commercial base oil obtained by Infineum using the HFRR apparatus depicted in Fig. 10.

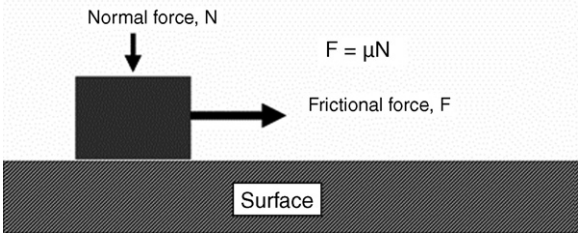

Fig. 9. The friction coefficient (μ) is defined as the ratio of normal force (N) to frictional force (F).

2. Methodology for constant NVT simulations

It was intended to model the behaviour of a film of fatty ester molecules at a finite temperature and at an interface between a hydrophilic surface and a hydrophobic liquid, so that the interactions defining friction reduction could be investigated [13,14].

It is assumed, based on the relative acidity of acids and alcohols (see Appendix 3), that as alcohols are very weakly acidic, little dissociation will occur so that the most significant mode of interaction with the hydroxylated metal oxide surface will be by the formation of hydrogen bonds [15].

All of the calculations in this work were performed on a SGi Octane with a single 250 MHz processor using Cerius2 software [16]. We employed the polymer consistent force field (hereafter referred to as PCFF), a member of the consistent force field family and a precursor to the COMPASS force field [17–23]. These force fields were originally developed for condensed phase simulations of organic polymers. We used modified torsion parameters similar to those proposed by Blomqvist et al. for the carboxyl torsion angles and the parameters shown in Table 1 for the O–C–C–H torsion in the glycerol moiety [24–26]. Non-bonded interactions were truncated over the interval 8.5–9 Å using a spline function. Periodic boundary conditions were used to model a condensed phase and in order to avoid problems associated with the artificial periodicity of the model care was taken to ensure that that the lengths of the simulation box were greater than twice the cut-off radius r_c [13,14,27,28].

The positions and the velocities were calculated using the Verlet Algorithm for the first time step and then the Leap-Frog Algorithm for all the subsequent time steps [29,30]. In all of the simulations in this work the default setting of 1×10^{-3} ps was used for the step size and a list of neighbouring atoms lying with 10 Å was compiled every 10 MD time steps [13].

In this work molecular dynamics (MD) simulations have been performed firstly under conditions of constant volume and temperature (NVT) and secondly under conditions of constant temperature and pressure (NPT). The method used for control of temperature and pressure was the Berendsen *weak coupling* method [31].

Goethite (α-FeOOH) was chosen to represent an oxidized steel surface because the surface functionalities of iron oxide are hydroxyl groups and because goethite is one of the more stable iron oxide hydroxides and is the one of the more common end products of corrosion and transformation [32].

Table 1
Torsion parameters used to treat the O–C–C–H torsion angles in the glycerol moiety

$k1$	$k2$	$k3$
−0.2731	1.3211	−1.080

Default atom types were assigned to crystalline goethite using the atom typing rules in Cerius2. The crystal was then cleaved parallel to the *bc* plane to generate a 10 Å thick 2D periodic surface cell of dimensions $u = 9.953$ Å, $v = 3.024$ Å and $\theta = 90°$ [16]. This surface was chosen as we believed that a low Miller index section through goethite would give a reasonable approximation to a lightly oxidized iron surface. This particular plane had hydroxyl groups perpendicular to the plane of the surface and so we believed it to be the most appropriate choice for a model. The aim of this work was to study the interactions of the ester molecules with lightly oxidized/hydrated iron surfaces. Surfaces with coordinatively unsaturated iron atoms are therefore not representative and so these were deleted to give a surface covered with oxo and hydroxyl groups. The stoichiometry of the resulting surface was H:O:Fe 1:2.25:1 and so it was necessary to scale the partial atomic charges using the charge equilibriation module to give a net charge of zero. While it would be desirable to saturate the surface with hydroxyl groups to the surface this was not done because we were not confident in that PCFF was sufficiently parameterized to deal with a mineral. A crystalline lattice was generated using the crystal builder module in Cerius2 and a ''super cell'' was constructed from this with the *a* and *b* axes as integral multiples of the unit cell lengths of crystalline

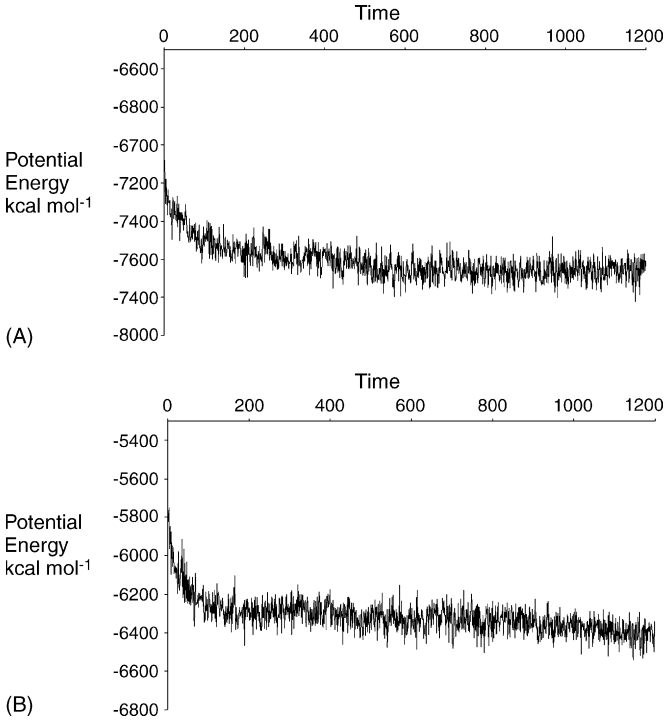

Fig. 10. Potential energy profile of the constant NVT simulations for: (A) 1-moctg and (B) 1,3-doctg.

Table 2
Details of the molecular dynamics simulations for 1-moctg and 1,3-doctg

Conditions	Constant NVT		Constant NPT	
Fixed cell dimensions, *a*, *b*, *c* (Å); *α*, *β*, *γ* (°)	19.906, 18.1434, 50.0; 90, 90, 90	19.906, 18.1434, 61.0; 90, 90, 90	Variable—see Fig. 20	Variable—see Fig. 20
Density of organic region (g cm^{-3})	0.91	0.93	0.92	0.91
Number of hexane solvent molecules	24	24	32	24
Ester	24 1-moctg molecules (12 on each face of the mineral surface)	24 1,3-doctg molecules (12 on each face of the mineral surface)	32 1-moctg	24 1,3-doctg
No. of atoms	1840	2232	1820	1920
Temperature (K)	700	700	300	300
Run time (ps)	1200	1200	3000	3000
Real time	8 days	10 days	Approximately 1 month	Approximately 1 month

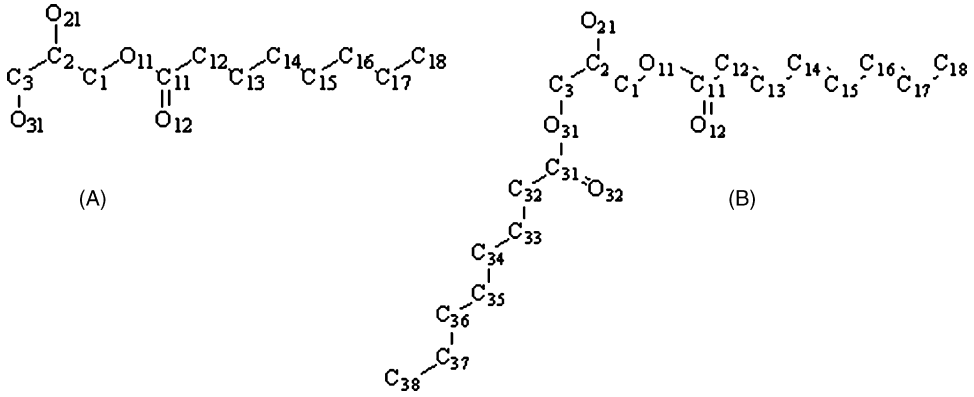

Scheme 1. Numbering scheme for the non-hydrogen atoms in (A) 1-monooctyl glycerol (1-moctg) and (B) 1,3-dioctyl glycerol (1,3-doctg) used in this work. Hydrogen atoms on carbons are numbered with a letter following the number of the preceding carbon, thus the hydrogen atoms on C2 are H2A and H2B. Hydrogen atoms on oxygen atoms use the same number as the parent atom so the hydrogen on O21 is named H21.

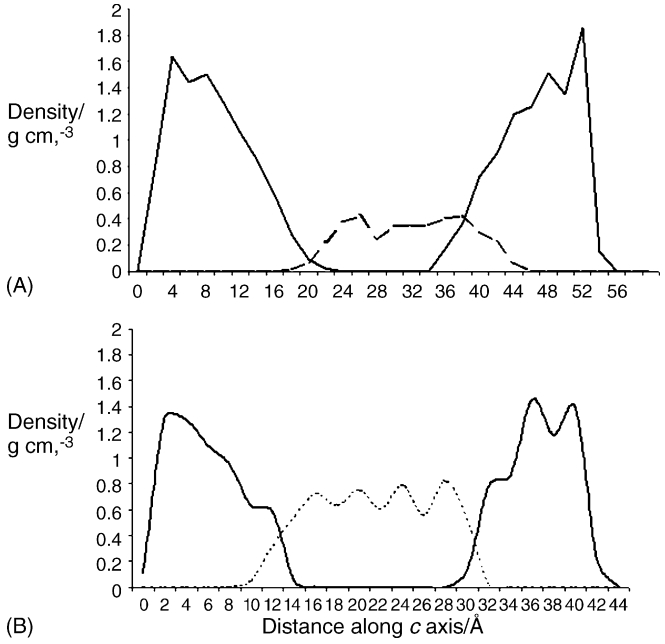

Fig. 11. Average density profile calculated at 50 ps intervals associated with the (A) 1,3-doctg and (B) 1-moctg systems. The ester density is shown as a solid line while the hexane density is shown as a dashed line.

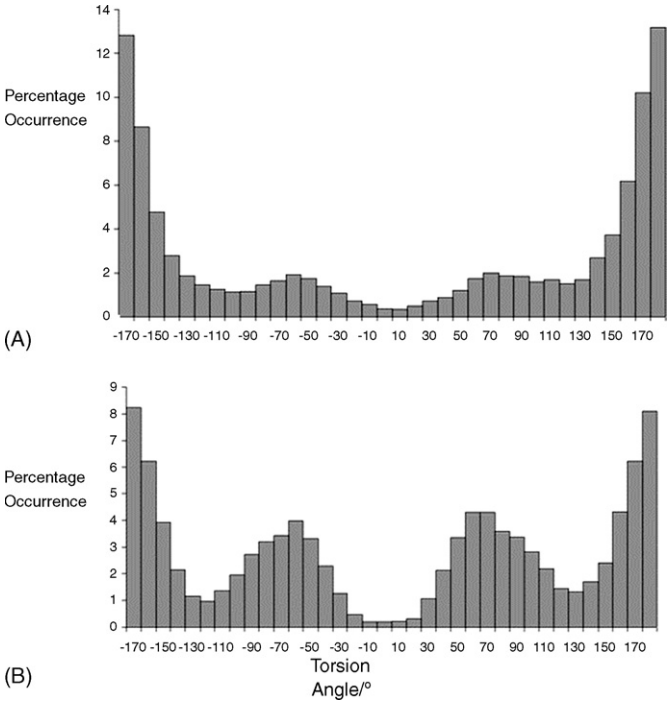

Fig. 12. Histogram showing the distribution of C–C–C–C torsion angles over the final 200 ps of the constant NVT molecular dynamics simulations for (A) 1,3-doctg and (B) 1-moctg molecules.

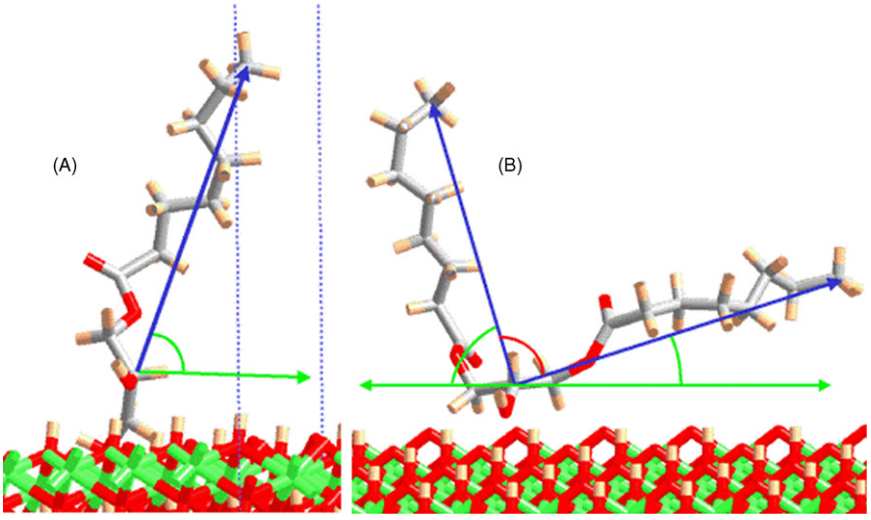

Fig. 13. Illustration of (A) C2–C18 tail length vector and angle to *ab* plane in 1-moctg and (B) C2–C18 and C2–C38 tail length vectors, angle between tail vectors and angle to *ab* plane in 1,3-doctg.

goethite. In order to simplify the calculations the positions of the atoms in the goethite lattice were constrained. The atom types and assigned charges for the goethite lattice are available in Appendix 4.

In order to make the calculations more manageable 1-monooleyl glyceride (1-moctg) and 1,3-di-oleyl glyceride (1,3-doctg) were chosen as models for 1-mog and 1,3-dog while hexane was used as a model for the C_{30} base lubricant used in commercial additive packages.

Simulations were performed in order to make comparisons about the respective surface activities of 1-moctg and 1,3-doctg molecules. The *c* axis was varied to make the models of the same density. The potential energy of the systems was plotted as a function of time and used to decide if the system was equilibrated.

Two models were constructed (Table 2) containing equal numbers of 1-moctg and 1,3-doctg molecules using the atom-labelling illustrated in Scheme 1. The models were created by setting the torsion angles in the ester molecule tail groups to 180° and placing them at the goethite surface. The positions of the atoms making up the goethite were constrained. After this the

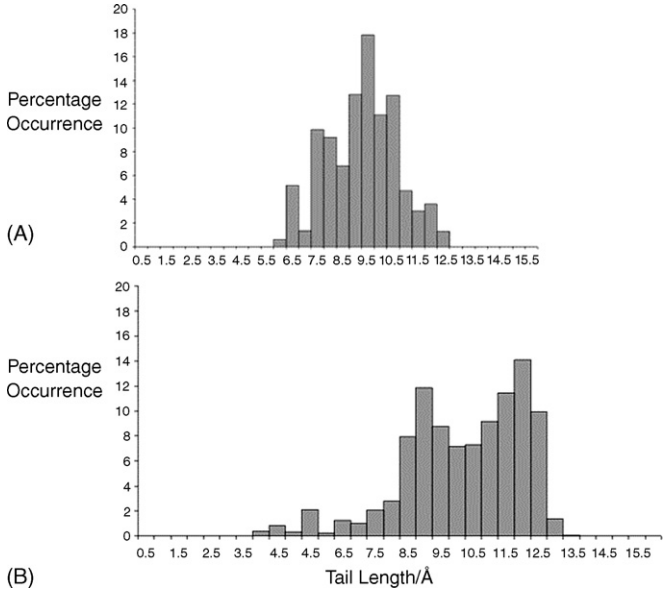

Fig. 14. Histogram showing the distribution of (A) C2–C18 distance in 1-moctg and (B) C2–C18 and C2–C38 distances in 1,3-doctg molecules over the final 200 ps of the constant NVT molecular dynamics simulation.

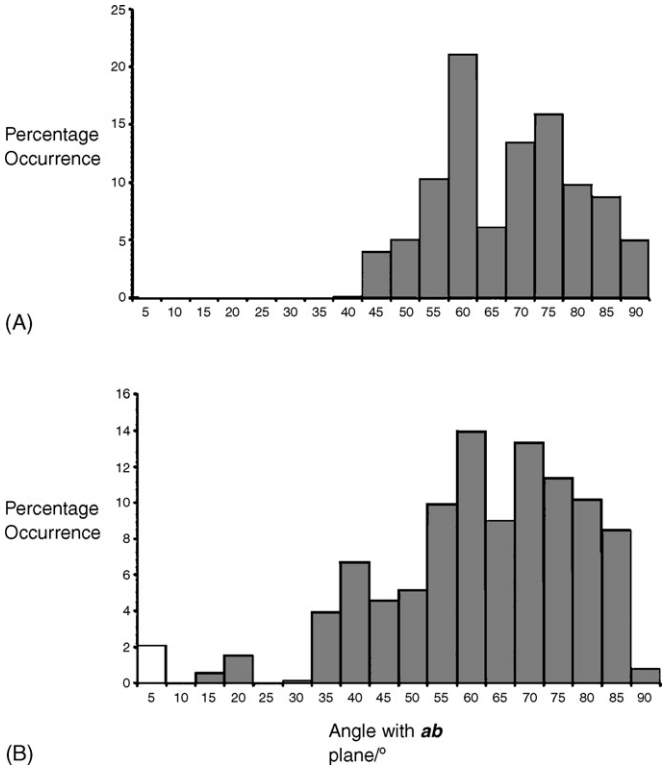

Fig. 15. Histogram showing the distribution over the final 200 ps of the constant NVT molecular dynamics simulation of the angles with the *ab* plane made by the (A) C2–C18 vectors of the 1-moctg molecules and (B) the C2–C18 and C2–C38 vectors of the 1,3-doctg molecules.

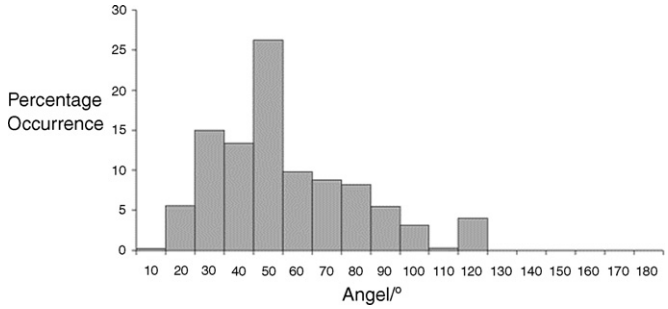

Fig. 16. Histogram showing the distribution of angles between the C2–C18 and C2–C38 tail vectors in 1,3-doctg molecules over the final 200 ps of the constant NVT molecular dynamics simulation.

energy of the model was minimised. An initial molecular dynamics run of 2 ps at 1400 K was carried out under constant NVE conditions with the velocities being rescaled every 0.5 ps, after which the energy of the model was again minimised [33]. Following this we performed a molecular dynamics simulation on the two systems described in Table 2.

The atomic positions and velocities for each of the simulation were written to a trajectory file every 1000 steps (1 ps). Analyses of the potential energy in the trajectory files are shown in Fig. 10(A and B), respectively. In the 1-moctg model the potential energy drops rapidly for the first 200 ps before declining gently between 200 ps and 800 ps. It was decided to deem the system equilibrated after the first 1000 ps and study the system over the final 200 ps. The 1,3-doctg system appears to equilibrate more slowly although the potential energy drops rapidly at the outset and it is still decreasing over the last 200 ps. The fluctuations in the potential energy (Fig. 10) could arise from a number of sources and are generally expected [13]. Berendsen et al. reported fluctuations of approximately 30 kJ mol^{-1} in the potential energy of a system of 216 water molecules when the weak coupling thermostat was employed to control the temperature [31]. In order to ensure that the trajectory files

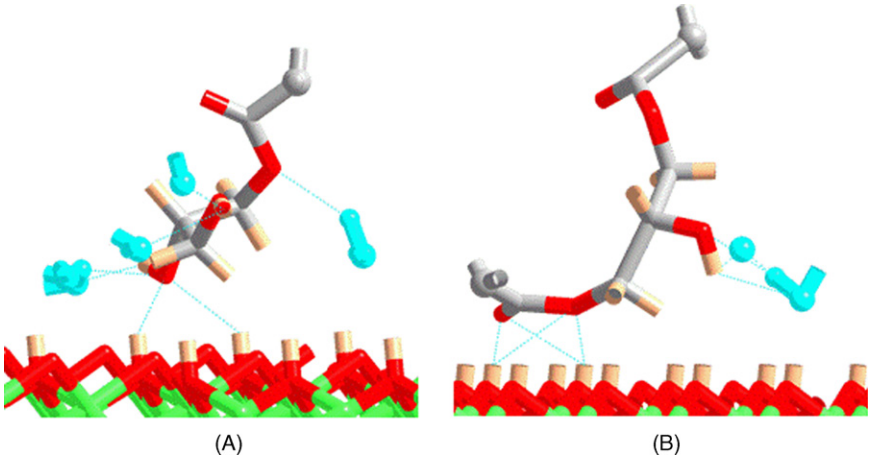

Fig. 17. Snapshot from the simulations showing examples of the hydrogen bonded interactions made by the head groups of (A) 1-moctg and (B) 1,3-doctg at the goethite surface. Hydrogen bonds are shown as dashed blue lines. Atoms in neighbouring ester molecules that are involved in hydrogen bonding are shown in blue.

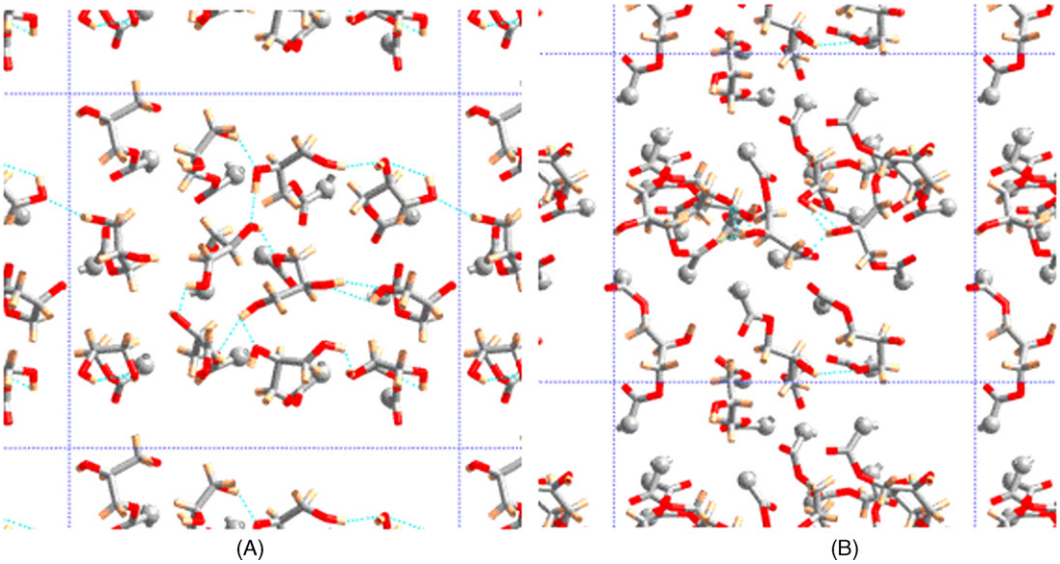

Fig. 18. Snapshots from molecular dynamics simulations showing intermolecular hydrogen bonded interactions between (A) 1-moctg and (B) 1,3-doctg molecules at the goethite surface. Atoms and interactions with atoms other than those in the "head group" have been omitted for clarity.

were of a manageable size, the details of the simulations presented here were only written to trajectory file once per 1000 steps. Consequently the profiles are discontinuous.

3. Discussion of constant NVT simulations

Analysis of the density due to ester and hexane, respectively, for each of the two systems (Fig. 11(A and B)) gives fairly similar results. In both there was a relatively high density near the metal surface due to the head group and a region of overlap of hexane and ester due to mixing of the tail groups and the solvent. Undulations in the curves are probably a result of the small system size and short sampling period.

Examination of the conformation adopted by the different torsion angles in the ester molecules shows that both molecules adopt similar conformations for related torsion angles (Fig. 12(A and B)) although it is notable that the distribution of torsion angles in this case is much broader than would be expected for the distributions in crystal structures. This is largely what would be expected from a distribution of torsion angles in a liquid system at an elevated temperature.

We defined (Fig. 13) the distance between the central atom (C2) and the last atom in the tail group (C18 in 1-moctg and C18 and C38 in 1,3-doctg) as a vector in an attempt to quantify the orientation and length of the ester molecules. The distributions of lengths and orientations of these vectors are shown in Figs. 14 and 15.

It is notable that the average lengths of the C2–C18 and C2–C38 vectors are larger for the 1,3-doctg molecules than the C2–C18 vector in the 1-moctg molecules. This is probably due to the incomplete coverage of the surface by the 1-moctg molecules which allows less efficient packing of the tail groups. It is interesting to see (Fig. 16) that there is always an angle between the C2–C18 and C2–C38 vectors in the 1,3-diester molecules which gives them a ‘‘forked’’ shape.

Visual inspection of the interactions made by the 1-moctg molecules shows that 12 and 10 ester molecules form hydrogen bonding interactions with the upper and lower surfaces of the goethite, respectively, while 7 and 8 molecules of 1,3-doctg are involved in hydrogen bonding interactions with the upper and lower surfaces.

For both 1-moctg (Fig. 17(A)) and 1,3-doctg (Fig. 17(B)) the hydroxyl groups on the goethite surface act principally as hydrogen bond donors to the ester molecules. The 1-moctg molecules form more hydrogen bonds to hydroxyl groups in neighbouring ester molecules (shown in blue in Fig. 17) than 1,3-doctg.

Snapshots from the molecular dynamics simulations for 1-moctg (Fig. 18(A) and 1,3-doctg (Fig. 18(B)) looking at the hydrogen bonds formed show that there are significantly more intermolecular interactions between the head groups of 1-moctg molecules than between the head groups of the 1,3-doctg molecules. It is also seen that in films of 1-moctg molecules the hydrogen bonds give chain like arrangements while when intermolecular hydrogen bonds do occur in 1,3-doctg they give rise to dimers.

The arrangement of hydrogen bonds in the 1-moctg simulations is consistent with the tendency of hydroxyl groups to simultaneously accept and donate hydrogen bonds, which has been shown to give rise to chains and helices in the crystal structures of sterically unhindered primary alcohols [34]. A film of 1-moctg molecules with an extended network of hydrogen bonds would be expected to be more stable than a film of 1,3-doctg molecules where hydrogen bonding is limited to intramolecular and dimeric interactions.

Using the arguments of Beltzer and Jahanmir, molecules related to 1-moctg would be expected to give a lower friction coefficient than those related to 1,3-doctg [4–7]. This is in agreement with the experimental data.

It has been shown that it is possible to use a molecular dynamics based methodology to investigate the relationship between structure and activity of organic friction modifiers. This is important because although their friction-reducing ability can readily be measured it is currently very difficult to investigate how the molecules are orientated and interact both with each other and with the surface being lubricated. This

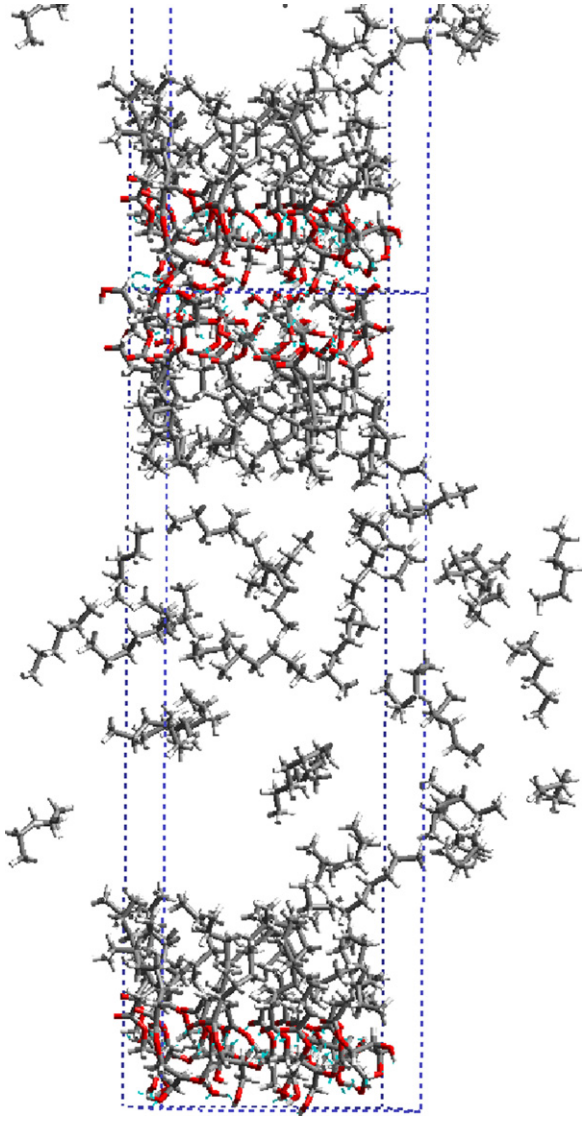

Fig. 19. Setup for NPT simulations. One computational box is shown together with the part of one immediate neighbour.

methodology could be used for the design of a series of new additive molecules.

4. Methodology for constant NPT simulations

The objectives were to perform simulations to study the packing and intermolecular interactions of ester molecules in a film and to make quantitative estimates of the area occupied at the interface by the 1-moctg and 1,3-doctg molecules. The limitations of PCFF in terms of under-estimating densities in molecular dynamics simulations at finite temperatures have been reported previously [17]. These errors arise because although the experimental data used to derive the parameters for the force field were obtained at finite temperature the parameters were developed based on static simulations corresponding to a classical state at 0 K. Although the surface areas occupied by 1-moctg and 1,3-doctg are calculated it is the relative differences that are of interest.

The systems described in Table 2 were built and minimised. The ester molecules were arranged in a bilayer with the hydrophilic head groups of one layer interacting with those in the layer below (Fig. 19). The bilayers were separated by hexane solvent molecules. 3D periodic boundary conditions

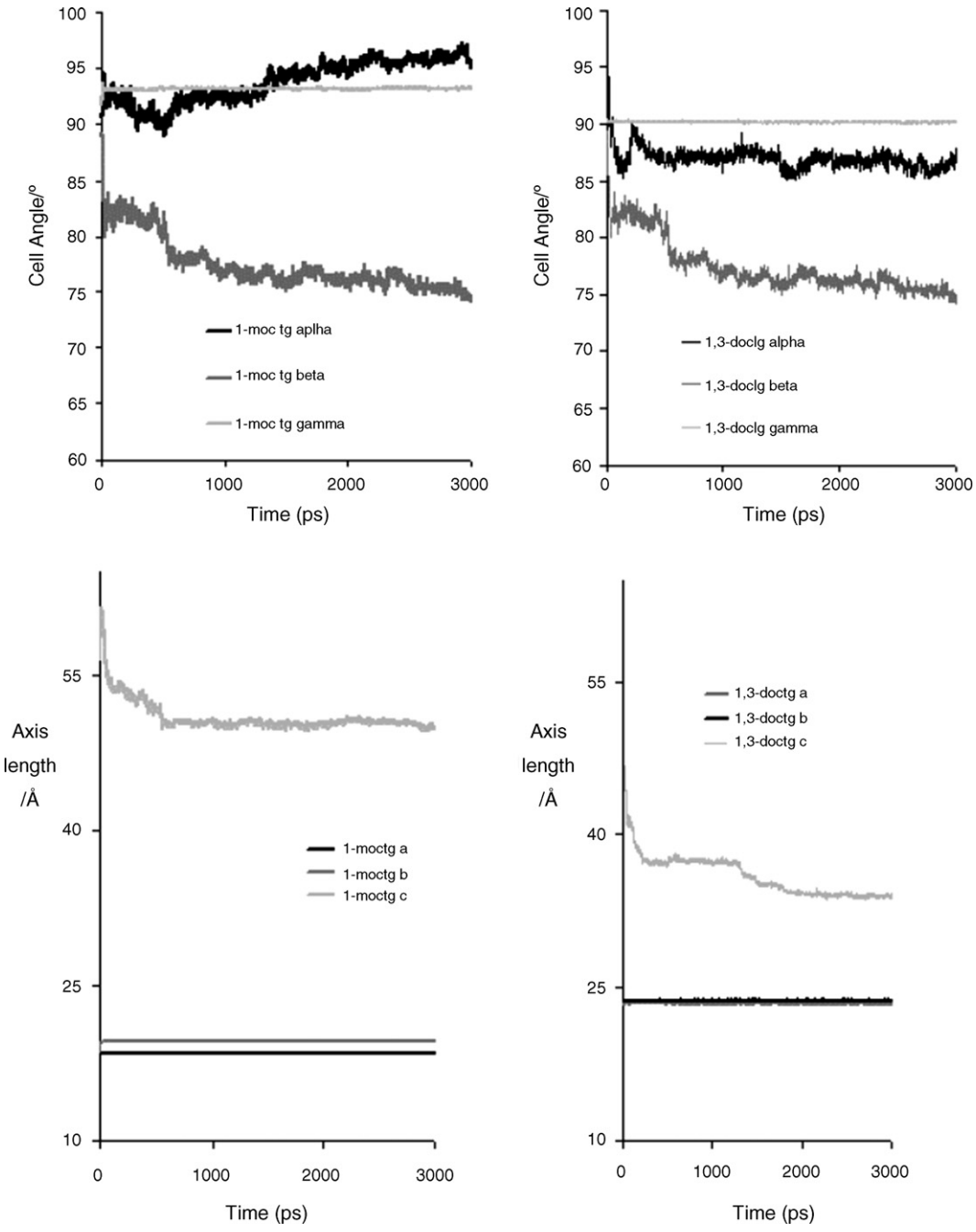

Fig. 20. Profile of the lengths and angles of the computational box in 1-moctg and 1,3-doctg constant NPT simulations.

were imposed. This "bilayer" arrangement was chosen to investigate the packing of the ester molecules at a hydrophilic surface. It would not have been feasible to use a crystalline substrate as changes in the cell dimensions a, b and γ to allow closer packing of the ester molecules would be impossible. The use of a molecular liquid such as water was considered but was felt to be inappropriate as there was a significant possibility that the head groups of the ester molecules would become buried in the water and would not interact with each other. This situation would not reflect the conditions occurring at the ester–goethite interface.

The hexane and ester molecules were arranged with their major axis perpendicular to the *ab* plane and the C–C–C–C torsion angles were set at 180°. Care was taken to ensure that all lengths of the sides of the computational box exceeded 18 Å. Initial MD runs of 7.5 ps were performed at 1400 K under NPT conditions using the Berendsen weak coupling thermostat to maintain temperature and pressure [31]. The temperature of the bath was then reduced to 300 K and molecular dynamics simulations were performed with the aim of equilibrating the system. The positions and velocities of the atoms in the system were written to a trajectory file every 1000 steps (1 ps) and the potential energy and volume of the two systems were analysed over the course of the simulations in order to ascertain whether or not the system had equilibrated.

The potential energy profiles for the 1-moctg and 1,3-doctg simulations (Appendix 5) show an initial rapid drop in potential energy, in part due to the transition from 1400 K to 300 K temperature. After this there was a longer, much slower drop in potential energy. Close inspection of the potential energy profiles shows that the energy is still slowly decreasing, even after 3000 ps. There was some concern whether the simulation had sampled enough phase space to enable the average area occupied by each ester molecule at the interface to be calculated. However, we believe that the simulations have been extensive enough to give a reasonable estimate of the relative areas occupied by the 1-moctg and 1,3-doctg molecules.

The lengths of, and the angles between, the edges of the computational box are shown over the course of the simulation in Fig. 20. It is apparent that there is very little change in a, b and γ over the course of the simulation. The consequence of this is that the area of the interface, and hence the average area occupied by each 1-moctg or 1,3-doctg molecule (Fig. 21), remains unchanged. The change in c, α and β corresponds to more efficient packing of the hexane solvent molecules and the 1-moctg and 1,3-doctg tail groups.

The average surface areas per molecule were calculated as an average over the last 100 ps of the simulation and are presented along with a snapshot of the hydrogen bonded interactions between 1-moctg and 1,3-doctg "head groups" in Table 3 and Fig. 22. The 1,3-doctg molecules occupy approximately twice the area at the interface of the 1-moctg molecules. This appears to be related to their ability to form intermolecular hydrogen bonds, which will in turn have a significant effect on surface activity and friction-modification properties as it reduces the stability of the adsorbed film.

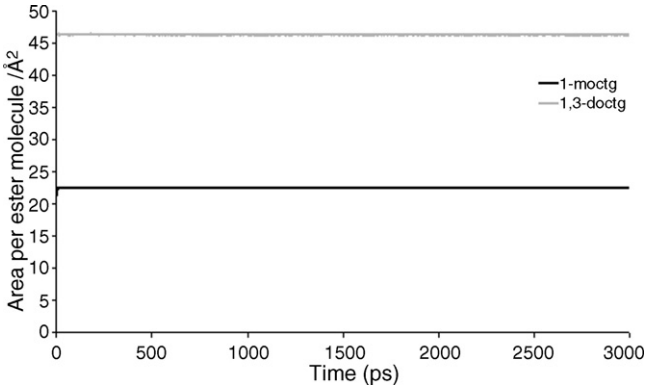

Fig. 21. Profile of the area occupied by each ester molecule in 1-moctg and 1,3-doctg constant NPT simulations.

There was little change in the area occupied by the 1-moctg molecules over the course of the MD simulation (Fig. 21). In order to establish that they were not in a local minimum it was decided to take the end product of the 1-moctg simulation and try simulated annealing. In this the temperature was incrementally raised from 300 K to 1500 K and then gradually lowered to 300 K over 500 ps. The intention was that raising the temperature would allow any potential energy barriers such as the stable arrangement of hydrogen bonds between the 1-moctg head groups to be crossed. In practice there was very little change in the area (approximately 1%) occupied by the ester molecules (Appendix 6). The disadvantage of this method is that the c axis becomes vastly elongated as it is dependent on weak interactions between the octyl tail groups and hexane molecules.

Other work in the literature suggests that the bulk properties of molecules are sensitive to the cut-off radius used for the non-bonded interactions and so we were concerned about truncating the non-bonded interactions at 9 Å. Vattulainen and co-workers studied [35] the effect on using different cut-off radii of 18 Å, 20 Å and 25 Å and the particle mesh Ewald technique to treat the non-bonded interactions on the bulk properties of a bilayer composed of 128 DPPC (Fig. 23) and 3655 water molecules over a 20 ns simulation. Even with large cut-off radii of 25 Å artificial ordering of atoms occurred in the simulations and the area occupied by each lipid molecule changed with the different cut-off radii. These artefacts were absent when the particle mesh Ewald method was used although this has limitations associated with exaggerating the periodicity of the system [14,35]. In this work it was impractical to use Ewald techniques because of the computational time required.

The most appropriate continuation of this work would be to test the sensitivity of the NPT simulations to the tail group of the surfactants by comparing simulations and experimental data

Table 3
The average surface area occupied by 1-moctg and 1,3-doctg in the constant NPT simulations

Solvate	Average area per molecule (Å^2)
1-moctg	22.5
1,3-doctg	46.13

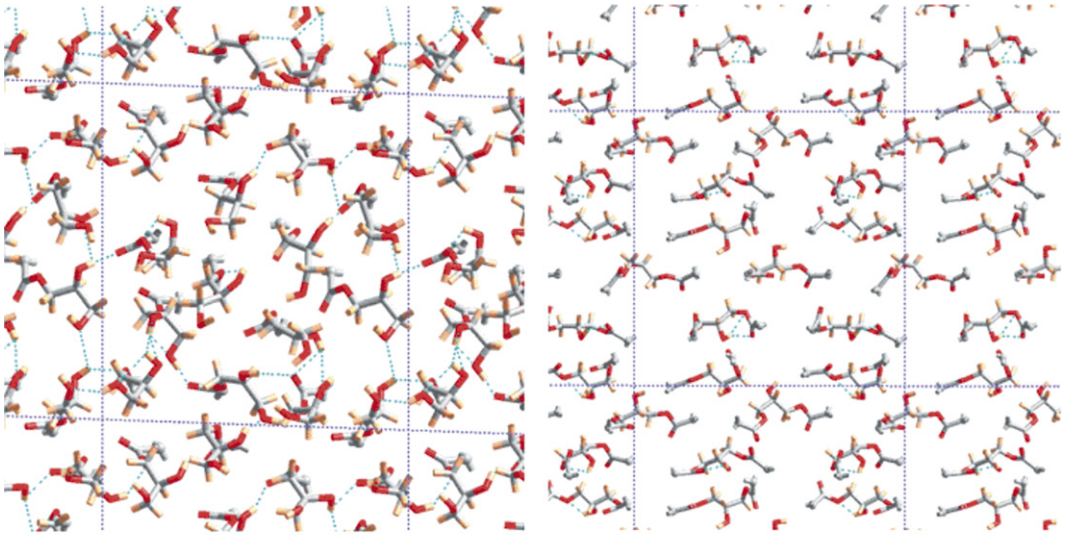

Fig. 22. (a and b) Snapshot of the lateral interactions between the headgroups of the 1-moctg and 1,3-doct molecules in the *ab* plane.

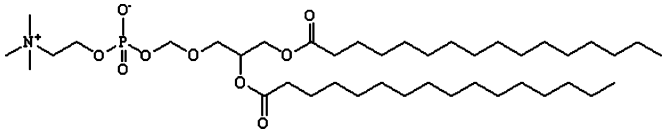

Fig. 23. Di-palmitoyl phosphatidyl choice, DPPC.

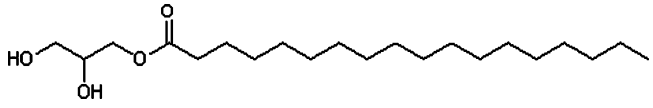

Fig. 24. 1-Mono-stearyl glycerol (1-msg).

for 1-mog (Fig. 6(A)) and 1-msg (Fig. 24) as the double bond in the tail group should have a significant effect on the stability of the film.

5. Conclusions

Molecular dynamics simulations have been shown to provide a useful *qualitative* analysis of the orientation, hydrogen bonding and packing of 1-moctg and 1,3-doctg molecules at a goethite surface and *quantitative* estimates of the area occupied by individual 1-moctg and 1,3-doctg molecules at an interface. Our computational results are consistent with experimental data and we believe the methodology presents the exciting possibility of being able to ‘‘screen’’ candidate molecules for use as organic friction modifiers in engine oils.

Acknowledgements

We thank Infineum UK Ltd. and the University of Edinburgh for a studentship (JED) and the Japanese Society for the Promotion of Science (JSPS) for additional funding.

Appendix A. Supplementary data

Supplementary data associated with this article can be found, in the online version, at doi:10.1016/j.jmgm.2006.03.006.

References

[1] B. Bhushan, Modern Tribology Handbook, CRC Press, London, 2001.
[2] R.W. Glyde, Chem. Br. 7 (1997) 39–41.
[3] R.M. Mortier, S. Orszulik, Chemistry and Technology of Lubricants, Chapman & Hall, London, 1997, p. 326.
[4] M. Beltzer, S. Jahanmir, ASLE Trans. 29 (1985) 423–430.
[5] M. Beltzer, S. Jahanmir, J. Tribol. 108 (1986) 109–116.
[6] M. Beltzer, S. Jahanmir, ASLE Trans. 30 (1) (1986) 47–54.
[7] M. Beltzer, J. Tribol. 114 (1992) 667–682.
[8] M.I. Temkin, J. Phys. Chem. (USSR) 1 (1941) 296–332.
[9] S.G. Harris, Ph.D. Thesis, University of Edinburgh, 1999.
[10] M. Frey, S.G. Harris, J.M. Holmes, D.A. Nation, S. Parsons, P.A. Tasker, R.E.P. Winpenny, Chem. Eur. J. 6 (2000) 1407–1415.
[11] M. Frey, S.G. Harris, J.M. Holmes, D.A. Nation, S. Parsons, P.A. Tasker, S.J. Teat, R.E.P. Winpenny, Angew. Chem. Int. Ed. 37 (1998) 3245–3248.
[12] J. McMurray, Organic Chemistry, Brooks/Cole Publishing Company, Monerey, CA, 1984.
[13] M.P. Allen, D.J. Tildesley, Computer Simulation of Liquids, Clarendon Press, Oxford, 1987.
[14] W.F. van Gunsteren, H.J.C. Berendsen, Angew. Chem. Int. Ed. Engl. 29 (1990) 992–1023.
[15] http://daecr1.harvard.edu/pdf/evans_pKa_table.pdf.
[16] Cerius2, Version 4.2, Molecular Simulations Inc., San Diego, 2000.
[17] H. Sun, J. Phys. Chem. B 102 (1998) 7338–7364.
[18] J.R. Maple, U. Dinur, A.T. Hagler, Proc. Natl. Acad. Sci. U.S.A. 85 (1988) 5350–5354.
[19] H. Sun, Macromolecules 26 (1993) 5924–5936.
[20] H. Sun, S. Mumby, J.R. Maple, A.T. Hagler, J. Am. Chem. Soc. 116 (1994) 2978–2987.
[21] H. Sun, J. Comput. Chem. 15 (1994) 752–768.
[22] H. Sun, S. Mumby, J.R. Maple, A.T. Hagler, J. Phys. Chem. 99 (1995) 5873–5882.
[23] H. Sun, Macromolecules 28 (1995) 701–712.

[24] J. Blomqvist, L. Ahjopalo, B. Mannfors, L.-O. Pietillä, J. Mol. Struct. (Theochem) 488 (1999) 247–262.
[25] J. Blomqvist, L. Ahjopalo, L.-O. Pietillä, J. Mol. Struct. (Theochem) 531 (2000) 359–374.
[26] J.E. Davidson, Ph.D. Thesis, The University of Edinburgh, 2005.
[27] E.A.V. Ebsworth, D.W.H. Rankin, S. Cradock, Structural Methods in Inorganic Chemistry, second ed., Blackwell Scientific Publications, Edinburgh, 1991, p. 343.
[28] T.A. Andrea, W.C. Swope, H.C. Andersen, J. Chem. Phys. 79 (1983) 4576–4584.
[29] L. Verlet, Phys. Rev. 159 (1967) 98–103.
[30] R.W. Hockney, Methods Comput. Phys. 9 (1970) 136–211.
[31] H.J.C. Berendsen, J.P.M. Postma, W.F. van Gunsteren, A. DiNola, J.R. Haak, J. Chem. Phys. 81 (1984) 3684–3690.
[32] R.M. Cornell, U. Schwertmann, The Metal Oxides, VCH, Cambridge, 1996.
[33] D.J. Tobias, M.L. Klein, J. Phys. Chem. 100 (1996) 6637–6648.
[34] C.P. Brock, L.L. Duncan, Chem. Mater. 6 (1994) 1307–1312.
[35] M. Patra, M. Karttunen, M.T. Hyvonen, E. Falck, P. Lindqvist, I. Vattulainen, Biophys. J. 84 (2003) 3636–3645.